MOLECULAR PHYSICS, 1997, VOL. 91, NO. 1, 145–160

Intermolecular interaction energies by topologically partitioned electric properties
II. Dispersion energies in one-centre and multicentre multipole expansions

By CHRISTOF HÄTTIG†§, GEORG JANSEN‡‖, BERND A. HESS†
and JÁNOS G. ÁNGYÁN‡

† Institut für Physikalische und Theoretische Chemie, Universität Bonn, Wegelerstrasse 12, D-53115 Bonn, Germany
‡ Laboratoire de Chimie théorique, Université Henri Poincaré, Unité de Recherche associée au CNRS 510, BP 239, F-54506 Vandœuvre-lès-Nancy, France

(*Received 16 September 1996; accepted 6 January 1997*)

Multicentre multipole expansions in principle should allow one to solve the 'shape' convergence problem arising in the calculation of long-range interaction energies between large non-spherical molecules via point-multipole expansions. In part I of this series (1996, *Molec. Phys.*, **88,** 69) it was shown that this indeed is the case for first-order electrostatic and second-order induction energies when employing distributed multipole moments and static polarizabilities generated from the topological partitioning of the molecular volume as provided by Bader's 'atoms-in-molecules' theory. Their generalization to frequency-dependent, topologically partitioned polarizabilities is used in the present contribution to compare the convergence behaviour of one-centre and multicentre multipole expansions of the second-order dispersion energy for homomolecular dimers of the water, carbon monoxide, cyanogen and urea molecules. The findings are similar to those for the induction energy; the radial 'extension' convergence problem, which already exists for point-multipole expanded interaction energies between atoms, necessarily persists, but the angular convergence problems linked to the shape of the interacting molecules can successfully be treated by multicentre multipole expansions of the dispersion energy.

1. Introduction

There are essentially two strategies to construct intermolecular interaction potentials. According to the first strategy, supermolecular calculations are performed. The interaction energy is calculated as the difference between the total energies of the complex and of the separated monomers, corrected for the basis set superposition error (BSSE) [1, 2]. The second strategy consists of accurate calculations of the charge distribution and response properties of the monomers; then the interaction energy is determined with the help of formulae derived from intermolecular perturbation theory [3–6]. Complete interaction potentials of high accuracy are quite difficult to obtain by either of the approaches. In the supermolecular method the evaluation of the dispersion energy necessitates expensive post-Hartree–Fock treatment of the complex, using large basis sets, which become prohibitive for the calculation of the high-dimensional potential surfaces for complexes consisting of polyatomic molecules. Calculations based on intermolecular perturbation theory may run into difficulties mostly in the evaluation of short-range interaction energy components, which requires an effort comparable with that of a supermolecular calculation when done accurately.

A reasonable compromise for the treatment of larger complexes is to combine Hartree–Fock interaction energies with dispersion energies determined from the dynamic multipole polarizabilities of the monomers [7] and corrected by suitable damping functions [7–10]. Unfortunately, for larger polyatomic molecules, the limitations of the one-centre multipole expansion underlying this method make it difficult to calculate the dispersion energy. A one-centre multipole expansion,

§ Present address: Department of Chemistry, Aarhus University, DK-8000 Aarhus C, Denmark.
‖ Present address: Institut für Theoretische Chemie, Universität Düsseldorf, Universitätsstrasse 1, D-40225, Düsseldorf, Germany.

0026–8976/97 $12·00 © 1997 Taylor & Francis Ltd.

which uses only one expansion site per monomer, is unable to describe the full complexity of the anisotropy of the charge density and of its response functions accurately. Moreover, it has quite poor convergence properties, especially for large non-spherical molecules. In fact, even when all the electrons of the monomers are confined to the interior of their respective van der Waals envelopes, the one-centre multipole expansion will diverge as soon as the smallest spheres around those envelopes start to overlap. This is a serious drawback for molecules which deviate strongly from spherical shape, for example, the chain-like *n*-alkanes or all-*trans*-alkenes. This specific problem of the one-centre multipole expansion of intermolecular interaction energies has been termed 'shape convergence problem' in part I [11] of this series.

As far as the electrostatic interaction energy is concerned the 'shape convergence problem' can be circumvented by multicentred (distributed) multipole expansions. In the practically important case when the wavefunction (and the charge density) is expanded in a basis of Gaussian-type basis functions, it is possible to calculate the exact multipolar limit of the electrostatic interaction energy [12–14], by considering the overlap multipole moments (OMMs), that is, all the (short) multipole expansions referred to the 'overlap centre' of the product of two Gaussian-type functions. Various partitionig schemes exist to redistribute the full set of OMMs on a reduced number of centres, leading to different distributed multipole moment (DMM) schemes [12–14].

In addition to the 'shape convergence problem', one should distinguish the 'extension convergence problem'. This difficulty, due to the exponential decay of the charge densities and of the associated charge-density susceptibility functions of the monomers, is independent of the shape of the system and exists already for spherically symmetric atoms. As a consequence of the 'extension convergence problem', multipole expansions of the interaction energy are only asymptotically convergent in the long-range limit and may diverge for each finite distance [15–20]. In the case of electrostatic interaction energies, this problem can be solved, for example, by replacing point multipole moments with so-called Gaussian multipole moments which incorporate the effect of the infinite extension of the monomer electronic charge densities [21].

In the case of the induction and dispersion contribution to interaction potentials the 'extension convergence problem' can be avoided in practice by multiplying the multipole expanded results with damping functions, which cut off the singularities of the multipole expansion, to mimic the non-expanded interaction [7–10].

The treatment of the 'shape convergence problem' necessitates a partitioning of the charge-density susceptibility functions of the monomers. Until very recently, there was no generally applicable partitioning scheme available that led to physically meaningful distributed multipole polarizabilities and could improve the convergence of expanded induction or dispersion energies. In particular, basis set partitioning schemes, similar to those used for DMMs, but also the more sophisticated Gauss–Hermite and smoothed Gauss–Hermite partitioning schemes derived by Le Sueur and Stone [22] led to distributed polarizabilities which are quite sensitive to basis set variations and result in unphysically large values of the charge–charge polarizabilities.

In part I [11] of this series we have shown that the convergence behaviour of the induction energy between dimers of non-spherical molecules drastically improves when using the recently developed topologically partitioned polarizabilities in multicentre multipole expansions [23]. The topologically partitioned electric properties (TPEPs) are obtained from a partitioning of the molecular volume into disjoint regions according to Bader's [24, 25] topological theory of 'atoms in molecules' and thus are parameter-free molecular properties with a well defined basis set limit.

The purpose of the present paper is to investigate the convergence behaviour of multipole expanded second-order dispersion energies, using frequency-dependent topologically partitioned polarizabilities up to high multipole ranks, and to demonstrate that the topological partitioning scheme leads to a significant improvement in the convergence behaviour for non-spherical polyatomic molecules. Furthermore, we present an efficient algorithm to evaluate dispersion interaction energies directly from frequency-dependent polarizabilities by avoiding the calculation of dispersion coefficients as intermediates. Thereby the scaling of both the CPU time and the storage requirements with the number of molecules, distribution sites and multipole components is reduced. This is an important point for the application of the TPEPs, which are designed for the calculation of interaction energies between large molecules with many atoms and expansion centres. In section 2, we review the one-centre and multicentre multipole expansion of the dispersion interaction energy and discuss the implemented algorithms.

To exemplify our results, homomolecular dimers of the same four molecules, which served as examples in our previous study on the electrostatic and the induction energy, will be used: water, carbon monoxide, cyanogen and urea. The majority of the geometrical configurations and technical details of the *ab-initio* distributed polarizability calculations are the same as in part I. Therefore the definition of the TPEPs and the necessary technical details are described only briefly in section 3. In section 4

we present and discuss the results of our calculations. Finally, in section 5, some general conclusions will be drawn.

2. Calculation of multipole expanded dispersion energies

Multipole expanded expressions for the dispersion energy are usually derived from the second-order intermolecular perturbation theory term for the non-expanded dispersion energy:

$$U_{\mathrm{disp}}^{(2)} = -\sum_{i\neq 0}\sum_{j\neq 0}\frac{|\langle\psi_i^{\mathrm{A}}\psi_j^{\mathrm{B}}|\hat{V}_{\mathrm{AB}}|\psi_0^{\mathrm{A}}\psi_0^{\mathrm{B}}\rangle|^2}{E_i^{\mathrm{A}} - E_0^{\mathrm{A}} + E_j^{\mathrm{B}} - E_0^{\mathrm{B}}}, \qquad (1)$$

where ψ_0^{X} and ψ_i^{X} denote the ground state and excited states of molecule X with energies E_0^{E} and E_i^{X}. The symbol $\sum\!\!\!\!\!\!\int$ indicates summation over discrete states and integration over continuum states. $\hat{V}_{\mathrm{AB}}$ is the electrostatic interaction potential operator between the molecules A and B, which can be written as

$$\hat{V}_{\mathrm{AB}} = \int\mathrm{d}\mathbf{r}\int\mathrm{d}\mathbf{r}'\hat{\rho}^{\mathrm{A}}(\mathbf{r})\frac{1}{|\mathbf{r}-\mathbf{r}'|}\hat{\rho}^{\mathrm{B}}(\mathbf{r}'), \qquad (2)$$

with the charge density operator $\hat{\rho}^{\mathrm{A}}$ defined as

$$\hat{\rho}^{\mathrm{A}}(\mathbf{r}) = \sum_{\alpha\in\mathrm{A}}\delta(\mathbf{r}-\mathbf{r}_\alpha)Z_\alpha - \sum_{i\in\mathrm{A}}\delta(\mathbf{r}-\mathbf{r}_i), \qquad (3)$$

and an analogous definition for $\hat{\rho}^{\mathrm{B}}$. Introducing the frequency-dependent charge-density susceptibility function

$$\alpha(\mathbf{r},\mathbf{r}'|\omega) = \sum_{i\neq 0}\frac{2(E_i-E_0)}{(E_i-E_0)^2-\omega^2}\langle\psi_0|\hat{\rho}(\mathbf{r})|\psi_i\rangle\langle\psi_i|\hat{\rho}(\mathbf{r}')|\psi_0\rangle \qquad (4)$$

and employing the integral transformation [26]

$$\frac{1}{(E_i^{\mathrm{A}}-E_0^{\mathrm{A}})+(E_j^{\mathrm{B}}-E_0^{\mathrm{B}})} = \frac{1}{2\pi}\int_0^\infty\mathrm{d}\omega\frac{E_i^{\mathrm{A}}-E_0^{\mathrm{A}}}{(E_i^{\mathrm{A}}-E_0^{\mathrm{A}})^2+\omega^2}\frac{E_j^{\mathrm{B}}-E_0^{\mathrm{B}}}{(E_j^{\mathrm{B}}-E_0^{\mathrm{B}})+\omega^2}, \qquad (5)$$

the unexpanded dispersion energy can be rewritten as a fivefold integral over the charge-density susceptibility functions of molecule A and B and two Coulomb interaction kernels [27]:

$$U_{\mathrm{disp}}^{(2)} = -\frac{1}{2\pi}\int_0^\infty\mathrm{d}\omega\int\mathrm{d}\mathbf{r}_1\int\mathrm{d}\mathbf{r}_1'\int\mathrm{d}\mathbf{r}_2\int\mathrm{d}\mathbf{r}_2'\,\alpha^{\mathrm{A}}(\mathbf{r}_1,\mathbf{r}_1'|\mathrm{i}\omega)\times\frac{1}{|\mathbf{r}_1-\mathbf{r}_2|}\frac{1}{|\mathbf{r}_1'-\mathbf{r}_2'|}\alpha^{\mathrm{B}}(\mathbf{r}_2,\mathbf{r}_2'|\mathrm{i}\omega). \qquad (6)$$

If one neglects the overlap between the charge-density susceptibility functions $\alpha^{\mathrm{A}}(\mathbf{r},\mathbf{r}'|\mathrm{i}\omega)$ and $\alpha^{\mathrm{B}}(\mathbf{r},\mathbf{r}'|\mathrm{i}\omega)$, the Coulomb interaction kernel $1/|\mathbf{r}_1-\mathbf{r}_2|$ can be expanded in a multipolar series, for example, in a series of real spherical tensors [28, 29]:

$$\frac{1}{|\mathbf{r}_1-\mathbf{r}_2|} = \sum_{\substack{l_{\mathrm{A}}\kappa_{\mathrm{A}}\\ l_{\mathrm{B}}\kappa_{\mathrm{B}}}} R_{l_{\mathrm{A}}\kappa_{\mathrm{A}}}^{\mathrm{A}}(\mathbf{r}_1)T_{l_{\mathrm{A}}\kappa_{\mathrm{A}}l_{\mathrm{B}}\kappa_{\mathrm{B}}}^{\mathrm{AB}}(\mathbf{r}^{\mathrm{AB}},\Omega_{\mathrm{AB}})R_{l_{\mathrm{B}}\kappa_{\mathrm{B}}}^{\mathrm{B}}(\mathbf{r}_2)$$
$$\text{for}\quad \|\mathbf{r}_1\|,\|\mathbf{r}_2\| \ll \|\mathbf{r}^{\mathrm{AB}}\|. \qquad (7)$$

The Coulomb interaction double tensors $T_{l_{\mathrm{A}}\kappa_{\mathrm{A}}l_{\mathrm{B}}\kappa_{\mathrm{B}}}^{\mathrm{AB}}$ depend on the distance vector $\mathbf{r}^{\mathrm{AB}} = \mathbf{r}^{\mathrm{A}} - \mathbf{r}^{\mathrm{B}}$ between the expansion centres of the two molecules and on their relative orientation Ω_{AB}. The $R_{l_{\mathrm{A}}\kappa_{\mathrm{A}}}^{\mathrm{A}}(\mathbf{r}) = R_{l_{\mathrm{A}}\kappa_{\mathrm{A}}}(\mathbf{r}-\mathbf{r}^{\mathrm{A}})$ denote real regular spherical harmonics.

When equation (7) is inserted into equation (6) and the fourfold integration over the variables $\mathbf{r}_1$, $\mathbf{r}_1'$, $\mathbf{r}_2$ and $\mathbf{r}_2'$ is carried out, one obtains the multipole expanded dispersion energy as a sum over frequency-dependent multipole–multipole polarizabilities and Coulomb interaction tensors:

$$U_{\mathrm{disp}}^{(2)} \approx U_{\mathrm{disp}}^{(2,\mathrm{MTP})} = -\frac{1}{2\pi}\int_0^\infty\mathrm{d}\omega\sum_{\substack{l_{\mathrm{A}}\kappa_{\mathrm{A}}\\ l_{\mathrm{B}}\kappa_{\mathrm{B}}}}\sum_{\substack{l_{\mathrm{A}}'\kappa_{\mathrm{A}}'\\ l_{\mathrm{B}}'\kappa_{\mathrm{B}}'}}\alpha_{l_{\mathrm{A}}\kappa_{\mathrm{A}}l_{\mathrm{A}}'\kappa_{\mathrm{A}}'}^{\mathrm{A}}(\mathrm{i}\omega)\times T_{l_{\mathrm{A}}\kappa_{\mathrm{A}}l_{\mathrm{B}}\kappa_{\mathrm{B}}}^{\mathrm{AB}}(\mathbf{r}^{\mathrm{AB}},\Omega_{\mathrm{AB}})\times T_{l_{\mathrm{A}}'\kappa_{\mathrm{A}}'l_{\mathrm{B}}'\kappa_{\mathrm{B}}'}^{\mathrm{AB}}(\mathbf{r}^{\mathrm{AB}},\Omega_{\mathrm{AB}})\alpha_{l_{\mathrm{B}}\kappa_{\mathrm{B}}l_{\mathrm{B}}'\kappa_{\mathrm{B}}'}^{\mathrm{B}}(\mathrm{i}\omega). \qquad (8)$$

Equation (8) can be reexpressed in terms of the dispersion integrals $X_{l_{\mathrm{A}}\kappa_{\mathrm{A}}l_{\mathrm{A}}'\kappa_{\mathrm{A}}'l_{\mathrm{B}}\kappa_{\mathrm{B}}l_{\mathrm{B}}'\kappa_{\mathrm{B}}'}^{\mathrm{AB}}$, by integrating over the frequency ω:

$$X_{l_{\mathrm{A}}\kappa_{\mathrm{A}}l_{\mathrm{A}}'\kappa_{\mathrm{A}}'l_{\mathrm{B}}\kappa_{\mathrm{B}}l_{\mathrm{B}}'\kappa_{\mathrm{B}}'}^{\mathrm{AB}} = \frac{1}{2\pi}\int_0^\infty\mathrm{d}\omega\,\alpha_{l_{\mathrm{A}}\kappa_{\mathrm{A}}l_{\mathrm{A}}'\kappa_{\mathrm{A}}'}^{\mathrm{A}}(\mathrm{i}\omega)\alpha_{l_{\mathrm{B}}\kappa_{\mathrm{B}}l_{\mathrm{B}}'\kappa_{\mathrm{B}}'}^{\mathrm{B}}(\mathrm{i}\omega), \qquad (9)$$

$$U_{\mathrm{disp}}^{(2,\mathrm{MTP})} = -\sum_{\substack{l_{\mathrm{A}}\kappa_{\mathrm{A}}\\ l_{\mathrm{B}}\kappa_{\mathrm{B}}}}\sum_{\substack{l_{\mathrm{A}}'\kappa_{\mathrm{A}}'\\ l_{\mathrm{B}}'\kappa_{\mathrm{B}}'}}T_{l_{\mathrm{A}}\kappa_{\mathrm{A}}l_{\mathrm{B}}\kappa_{\mathrm{B}}}^{\mathrm{AB}}(\mathbf{r}^{\mathrm{AB}},\Omega_{\mathrm{AB}})\times T_{l_{\mathrm{A}}'\kappa_{\mathrm{A}}'l_{\mathrm{B}}'\kappa_{\mathrm{B}}'}^{\mathrm{AB}}(\mathbf{r}^{\mathrm{AB}},\Omega_{\mathrm{AB}})X_{l_{\mathrm{A}}\kappa_{\mathrm{A}}l_{\mathrm{A}}'\kappa_{\mathrm{A}}'l_{\mathrm{B}}\kappa_{\mathrm{B}}l_{\mathrm{B}}'\kappa_{\mathrm{B}}'}^{\mathrm{AB}}. \qquad (10)$$

In the following, the formulation outlined in equations (7)–(10) and described at length by Stone and co-workers, will be called the uncoupled representation, because the interaction tensors $T_{l_{\mathrm{A}}\kappa_{\mathrm{A}}l_{\mathrm{B}}\kappa_{\mathrm{B}}}^{\mathrm{AB}}$ as well as the polarizabilities $\alpha_{lk\kappa'}$ have a double-tensor structure, that is, they do not transform as an irreducible representation of SO(3), but as a representation of the product group $\mathrm{SO}(3)\otimes\mathrm{SO}(3)$. The dispersion integrals $X_{l_{\mathrm{A}}\kappa_{\mathrm{A}}l_{\mathrm{A}}'\kappa_{\mathrm{A}}'l_{\mathrm{B}}\kappa_{\mathrm{B}}l_{\mathrm{B}}'\kappa_{\mathrm{B}}'}^{\mathrm{AB}}$ transform even as a representation of $\mathrm{SO}(3)\otimes\mathrm{SO}(3)\otimes\mathrm{SO}(3)\otimes\mathrm{SO}(3)$.

In applications, usually a coupled representation is used with irreducible polarizabilities and dispersion integrals, as derived for example by Wormer and co-workers [30, 31] and by Pack [32]. In this formulation

the polarizabilities and dispersion coefficients appear as irreducible tensors, and they are more closely related to experimental data and to expansion coefficients for the asymptotic long-range potentials of van der Waals complexes. For atoms and for highly symmetric molecules, there is also a considerably smaller number of non-vanishing irreducible polarizabilities and dispersion coefficients than there are dispersion integrals in the uncoupled representation. In particular, this is true for atom–atom and for atom–diatom van der Waals complexes where it is very convenient to calculate the dispersion energy via the irreducible dispersion coefficients.

For van der Waals complexes built from general asymmetric molecules, however, the number of irreducible dispersion coefficients becomes comparable with the number of uncoupled dispersion integrals. In this case it may be more efficient to calculate multipole expanded dispersion energies by the simple uncoupled expressions, because the coupling to irreducible tensors leads to additional computational overhead. The computational advantage of the uncoupled representation becomes decisive when the integral over the frequency in equation (8) is solved by a numerical quadrature scheme with a number of grid points ω_j that is small compared with the number of polarizability components considered;

$$U_{\mathrm{disp}}^{(2,\mathrm{MTP})} = -\sum_j W(\omega_j)\frac{1}{2\pi}\sum_{\substack{l_\mathrm{A}\kappa_\mathrm{A}\\ l_\mathrm{B}\kappa_\mathrm{B}}}\sum_{\substack{l_{\mathrm{A}'}\kappa_{\mathrm{A}'}\\ l_{\mathrm{B}'}\kappa_{\mathrm{B}'}}} \alpha^{\mathrm{A}}_{l_\mathrm{A}\kappa_\mathrm{A}l_{\mathrm{A}'}\kappa_{\mathrm{A}'}}(\mathrm{i}\omega_j) \times T^{\mathrm{AB}}_{l_{\mathrm{A}'}\kappa_{\mathrm{A}'}l_\mathrm{B}\kappa_\mathrm{B}}(\mathbf{r}^{\mathrm{AB}},\Omega_{\mathrm{AB}}) \times \alpha^{\mathrm{B}}_{l_\mathrm{B}\kappa_\mathrm{B}l_{\mathrm{B}'}\kappa_{\mathrm{B}'}}(\mathrm{i}\omega_j) T^{\mathrm{BA}}_{l_{\mathrm{B}'}\kappa_{\mathrm{B}'}l_\mathrm{A}\kappa_\mathrm{A}}(\mathbf{r}^{\mathrm{BA}},\Omega_{\mathrm{BA}}). \quad (11)$$

Then the summation over polarizability components can be factorized, and it is computationally much more efficient to calculate the dispersion energy for each geometry directly from the frequency-dependent polarizabilities and to avoid the intermediate use of dispersion integrals. This is achieved by evaluating frequency-dependent **S** tensors:

$$S^{\mathrm{AB}}_{l_\mathrm{A}\kappa_\mathrm{A}l_\mathrm{B}\kappa_\mathrm{B}}(\mathbf{r}^{\mathrm{AB}},\Omega_{\mathrm{AB}},\omega) = \sum_{\substack{l_{\mathrm{A}'}\kappa_{\mathrm{A}'}\\ \mathrm{A}'}} \alpha^{\mathrm{A}}_{l_\mathrm{A}\kappa_\mathrm{A}l_{\mathrm{A}'}\kappa_{\mathrm{A}'}}(\mathrm{i}\omega) \times T^{\mathrm{AB}}_{l_{\mathrm{A}'}\kappa_{\mathrm{A}'}l_\mathrm{B}\kappa_\mathrm{B}}(\mathbf{r}^{\mathrm{AB}},\Omega_{\mathrm{AB}}), \quad (12)$$

which are subsequently contracted to yield

$$U_{\mathrm{disp}}^{(2,\mathrm{MTP})} = -\sum_j \frac{1}{2\pi} W(\omega_j) \sum_{\substack{l_\mathrm{A}\kappa_\mathrm{A}\\ \mathrm{A}}}\sum_{\substack{l_\mathrm{B}\kappa_\mathrm{B}\\ \mathrm{B}}} S^{\mathrm{AB}}_{l_\mathrm{A}\kappa_\mathrm{A}l_\mathrm{B}\kappa_\mathrm{B}}(\mathbf{r}^{\mathrm{AB}},\Omega_{\mathrm{AB}},\omega_j) \times S^{\mathrm{BA}}_{l_\mathrm{B}\kappa_\mathrm{B}l_\mathrm{A}\kappa_\mathrm{A}}(\mathbf{r}^{\mathrm{AB}},\Omega_{\mathrm{AB}},\omega_j). \quad (13)$$

To the best of our knowledge, this factorization has not been described in the literature before. In the coupled formulation such a factorization is impossible because, for example, the transformation of the polarizabilities to the irreducible representation involves both indices κ and κ'.

For a distributed multipole expansion the uncoupled formulation provides the only useful scheme to compute interaction energies, because the two index pairs $l\kappa$ and $l\kappa'$ are in general related to different expansion centres. Coulomb interaction tensors will also depend on different distance vectors. In the case of distributed multipole expansion the factorization of equations (12) and (13) becomes much more important, in particular, if there are more than a few expansion centres per molecule. The cost of the computation of dispersion energies via distributed dispersion integrals

$$X^{aa'bb'}_{l_a\kappa_a l_{a'}\kappa_{a'}l_b\kappa_b l_{b'}\kappa_{b'}} = \frac{1}{2\pi}\int_0^\infty \mathrm{d}\omega\, \alpha^{aa'}_{l_a\kappa_a l_{a'}\kappa_{a'}}(\mathrm{i}\omega)\alpha^{bb'}_{l_b\kappa_b l_{b'}\kappa_{b'}}(\mathrm{i}\omega), \quad (14)$$

$$U_{\mathrm{disp}}^{(2,\mathrm{MTP})} = -\sum_{\substack{a,a'\in\mathrm{A}\\ b,b'\in\mathrm{B}}}\sum_{\substack{l_{a'}\kappa_{a'}\\ l_b\kappa_b}}\sum_{\substack{l_a\kappa_a\\ l_{b'}\kappa_{b'}}} T^{ab}_{l_a\kappa_a l_b\kappa_b}(\mathbf{r}^{ab},\Omega_{\mathrm{AB}}) \times T^{a'b'}_{l_{a'}\kappa_{a'}l_{b'}\kappa_{b'}}(\mathbf{r}^{a'b'},\Omega_{\mathrm{AB}}) X^{aa'bb'}_{l_a\kappa_a l_{a'}\kappa_{a'}l_b\kappa_b l_{b'}\kappa_{b'}}, \quad (15)$$

scales as $O(N_{\mathrm{cent}}^4 \times L^8)$, where N_{cent} is the number of expansion centres a, a' and b, b' per molecule A and B, and L is the maximum rank of the multipole expansion. However, an even more serious bottleneck of this approach are the large storage requirements for the $\frac{1}{4}N_{\mathrm{cent}}^4 \times (L+1)^8$ dispersion integrals, that have to be kept in main memory or on disc. The expenditures for a computation along the lines of equations (12) and (13):

$$S^{ab}_{l_a\kappa_a l_b\kappa_b}(\mathbf{r}^{\mathrm{AB}},\Omega_{\mathrm{AB}},\omega) = \sum_{a'\in\mathrm{A}}\sum_{\substack{l_{a'}\kappa_{a'}\\ a'}} \alpha^{aa'}_{l_a\kappa_a l_{a'}\kappa_{a'}}(\mathrm{i}\omega) \times T^{a'b}_{l_{a'}\kappa_{a'}l_b\kappa_b}(\mathbf{r}^{a'b},\Omega_{\mathrm{AB}}), \quad (16)$$

$$U_{\mathrm{disp}}^{(2,\mathrm{MTP})} = -\sum_i \frac{1}{2\pi} W(\omega_j) \times \sum_{\substack{a\in\mathrm{A}\\ b\in\mathrm{B}}}\sum_{\substack{l_{a'}\kappa_{a'}\\ l_b\kappa_b}} S^{ab}_{l_a\kappa_a l_b\kappa_b}(\mathbf{r}^{ab},\Omega_{\mathrm{AB}},\omega_i) \times S^{ba}_{l_b\kappa_b l_a\kappa_a}(\mathbf{r}^{ab},\Omega_{\mathrm{AB}},\omega_i), \quad (17)$$

scale as $O(N_{\mathrm{freq}} \times N_{\mathrm{cent}}^3 \times L^5)$, if the tensors $\mathbf{S}^{ab}$ are evaluated by the recurrence relations proposed in [33]. If the number of grid points for the integration of ω is small compared with $N_{\mathrm{cent}} \times L^3$, this results in a significant saving of CPU time. In addition, this algorithm requires, beside some small auxiliary arrays, only storage of the $\frac{1}{2}N_{\mathrm{cent}}^2 \times (L+1)^4$ polarizabilities and two **S** intermediates of the size $(L+1)^4$.

In part I [11] of this series, where we studied electrostatic and induction energies calculated from topologically partitioned multipole moments and polarizabilities, we showed that the usually applied expansion of interaction energies in orders of the reciprocal intermolecular distance $1/|\mathbf{r}^{AB}|$ can easily give unphysical results for the induction energy. For the water dimer in a particular relative orientation, even positive induction energies have been obtained by this truncation scheme.

As an alternative approach we proposed to use the tensor rank as order parameter for multipole expansions. This expansion, which we called the 'maximum-rank expansion' or 'L expansion' to distinguish it from the '$1/R$ expansion' guarantees that the induction energy is always negative. Although it is true that the L expansion is not invariant with respect to identical translations of the expansion centres on A and B, in contrast with the $1/R$ expansion [34], this is not of much concern to the distributed expansion where the atomic nuclei provide natural expansion centres. In the regions of van der Waals minima the L expansion seems to be physically more justified than the $1/R$ expansion. Remember that for this intermediate distance range the multipole expanded interaction energies, especially the induction and the dispersion energy, must be pre-multiplied by exponentially decreasing damping functions to account for overlap effects in order to get realistic non-divergent results. In this case, one no longer has a well defined order parameter for the $1/R$ expansion, while the tensor rank is still a good order parameter. It turns out that, by a comparison of the two formalisms, the L expansion is also simpler to implement and it is even more efficient for the induction energy than the usually applied $1/R$ expansion.

Similar arguments hold for the dispersion energy. It can be shown that the L expansion scheme guarantees in each order of the expansion that the dispersion energy is negative. The reason for this property is that by the truncation of each multipole series at a common maximum rank L the approximation of an interaction energy through its Lth order corresponds to an approximation of the perturbation operator $\hat{V}_{AB}$ by its Lth order:

$$\left(\frac{1}{|\mathbf{r}-\mathbf{r}'|}\right)^{(L)} = \sum_{l_A=0}^{L}\sum_{\kappa_A}^{+l_A}\sum_{l_B=0}^{L}\sum_{\kappa_B}^{+l_B} R^{A}_{l_A\kappa_A}(\mathbf{r}) \times T^{AB}_{l_A\kappa_A l_B\kappa_B}(\mathbf{r}_{AB},\Omega_{AB}) R^{B}_{l_B\kappa_B}(\mathbf{r}'), \quad (18)$$

$$\hat{V}_{AB} = \sum_{l_A=0}^{L}\sum_{\kappa_A}^{+l_A}\sum_{l_B=0}^{L}\sum_{\kappa_B}^{+l_B} T^{AB}_{l_A\kappa_A l_B\kappa_B}(\mathbf{r}_{AB},\Omega_{AB}) \times \int d\mathbf{r}\, R^{A}_{l_A\kappa_A}(\mathbf{r})\hat{\rho}^{A}(\mathbf{r}) \int d\mathbf{r}'\, R^{B}_{l_B\kappa_B}(\mathbf{r}')\hat{\rho}^{B}(\mathbf{r}'). \quad (19)$$

Within the L expansion scheme it is thus possible to write the dispersion energy for each L as a second-order perturbation theory expression, which is always negative, provided that both molecules are in their ground states:

$$U^{(L)}_{disp} = -\sum_{i\neq 0}\sum_{j\neq 0}\frac{|\langle\psi^{A}_i\psi^{B}_j|\hat{V}^{(L)}_{AB}|\psi^{A}_0\psi^{B}_0\rangle|^2}{E^{A}_i - E^{A}_0 + E^{B}_j - E^{B}_0}. \quad (20)$$

A similar correspondence between the order of an approximation for the energy and an approximation for the interaction potential $\hat{V}_{AB}$ does not exist for the expansion in orders of $1/|\mathbf{r}_{AB}|$, with the exception of the first-order electrostatic energy.

The explicit expressions for the dispersion energy of order N in $1/R$ in a distributed multipole expansion along the lines of equations (16) and (17) are

$$S^{ab}_{[n]\kappa_a l_b\kappa_b}(\omega) = \sum_{a'\in A}\sum_{\kappa_{a'}}\alpha^{aa'}_{l_a\kappa_a,(n-l_b-1)\kappa_{a'}}(\omega)T^{a'b}_{(n-l_b-1)\kappa_{a'}l_b\kappa_b}, \quad (21)$$

$$U_{disp,N} = -\frac{1}{2\pi}\sum_j W(\omega_j)\sum_{n=1}^{N}\sum_{a\in A}\sum_{b\in B}\sum_{\substack{\kappa_a\\ l_b\kappa_b}} S^{ab}_{[n]\kappa_a l_b\kappa_b}(\omega_j) \times S^{ba}_{[n-1]l_b\kappa_b l_a\kappa_a}(\omega_j). \quad (22)$$

As for the induction energy, also for the $1/R$ expansion of the dispersion energy an additional index n must be introduced, to keep track of the order parameter in the intermediates. This complicates the loop structure and results in a significant computational overhead.

The analogous expressions for the L expansion are comparatively simply structured:

$$S^{ab}_{l_a\kappa_a l_b\kappa_b}(\omega) = \sum_{a'\in A}\sum_{l_{a'}=0}^{L}\sum_{\kappa_{a'}}\alpha^{aa'}_{l_a\kappa_a,l_{a'}\kappa_{a'}}(\omega)T^{a'b}_{l_{a'}\kappa_{a'}l_b\kappa_b}, \quad (23)$$

$$U_{disp,N} = -\frac{1}{2\pi}\sum_j W(\omega_j)\sum_{a\in A}\sum_{b\in B}\sum_{\substack{l_a\kappa_a\\ l_b\kappa_b}}^{L} S^{ab}_{l_a\kappa_a l_b\kappa_b}(\omega_j) \times S^{ba}_{l_b\kappa_b l_a\kappa_a}(\omega_j), \quad (24)$$

and as for the induction energy the additional index n, necessary for a truncation at a defined order in $1/R$, drops out.

3. Technical details

For all property calculations on the monomers we used Sadlej's [35] medium-sized polarization basis sets and experimental gas-phase geometries for the molecules H_2O, CO and NCCN [36–38]. For the urea monomer the planar geometry as found in the crystal [39] has been employed.

In the topological theory of 'atoms in molecules' the three-dimensional physical space is partitioned into disjoint atomic regions, Ω_0^a, defined by the condition that for the separating surfaces S^a the flux of the unperturbed electronic charge density $\rho(\mathbf{r})$ vanishes [24, 25]

$$\nabla\rho(\mathbf{r})\cdot\mathbf{n}(\mathbf{r}) = 0 \quad \text{for all } \mathbf{r} \in S^a. \tag{25}$$

This real-space partitioning is used to define atomic multipole integrals,

$$\langle p|\hat{Q}^a_{lm}|q\rangle = \int_{\Omega_0^a} \phi_p^*(\mathbf{r}) R_{lm}(\mathbf{r} - \mathbf{r}^a)\phi_q(\mathbf{r})\,\mathrm{d}\mathbf{r}, \tag{26}$$

which occur in the calculation of mean values as well as they enter in usual linear response programs to calculate (frequency-dependent) topologically partitioned polarizabilities [23]

$$\alpha^{aa'}_{lm,l'm'}(\omega) = \int_{\Omega_0^a} \mathrm{d}\mathbf{r} \int_{\Omega_0^{a'}} \mathrm{d}\mathbf{r}' R_{lm}(\mathbf{r} - \mathbf{r}^a) \times \alpha(\mathbf{r},\mathbf{r}'|\omega) R_{l'm'}(\mathbf{r}' - \mathbf{r}^{a'}). \tag{27}$$

Formally, the topologically partitioned multipole–multipole polarizabilities can be defined by multipole expansion of real-space partitioned charge-density susceptibility functions, which have non-vanishing values only for $\mathbf{r} \in \Omega_0^a$ and $\mathbf{r}' \in \Omega_0^{a'}$:

$$\alpha^{aa'}_{lm,l'm'}(\omega) = \int \mathrm{d}\mathbf{r} \int \mathrm{d}\mathbf{r}' R_{lm}(\mathbf{r} - \mathbf{r}^a) \times \alpha^{aa'}(\mathbf{r},\mathbf{r}'|\omega) R_{l'm'}(\mathbf{r}' - \mathbf{r}^{a'}), \tag{28}$$

$$\alpha^{aa'}(\mathbf{r},\mathbf{r}'|\omega) = \int_{\Omega_0^a} \mathrm{d}\mathbf{r}'' \int_{\Omega_0^{a'}} \mathrm{d}\mathbf{r}''' \, \delta(\mathbf{r} - \mathbf{r}'') \times \delta(\mathbf{r}' - \mathbf{r}''')\alpha(\mathbf{r}'',\mathbf{r}'''|\omega). \tag{29}$$

Very recently Cioslowski [40] defined distributed polarizabilities as the atomic-pair contribution to the molecular polarizabilities, calculated with relaxed atomic perturbation operators which incorporate the surface relaxation terms:

$$\alpha^{aa'}_{V,W} = \sum_{n\neq 0} \left(\frac{\langle \Psi_0|V_a^{rlx}|\Psi_n\rangle\langle\Psi_n|W_{a'}^{rlx}|\Psi_0\rangle}{E_n - E_0} + \frac{\langle \Psi_0|W_a^{rlx}|\Psi_n\rangle\langle\Psi_n|V_{a'}^{rlx}|\Psi_0\rangle}{E_n - E_0} \right). \tag{30}$$

Owing to the incorporation of the surface terms, the relaxed atomic perturbation operators V_a^{rlx} depend in a nonlinear way on all external fields applied to the molecule and different terms enter to the relaxed operators in each order of response theory. The properties obtained by this definition describe the responses of atoms in molecules including the relaxation of the interatomic surfaces but, in contrast with the topologically partitioned response properties defined by equation (27) and analogous equations for higher-order responses, they do not provide a real-space partitioning of the respective molecular response function similar to equations (28)–(29). However, both approaches provide a consistent picture of the charge-density response and conserve the total polarizabilities as well as the invariance with respect to an interchange of the perturbation operators.

The atomic multipole integrals required for the calculation of the distributed polarizabilities were provided by a modified version of the 'PROAIM' program [41] as described in part I. The frequency-dependent polarizabilities were determined at the time-dependent coupled Hartree–Fock (TDHF) level of theory using the programs 'CAUCHY' [42] and 'FOURIER' [43] which are interfaced to the 'MOLCAS-2' program package [44] to provide the self-consistent field wavefunction and the necessary two-electron integrals.

For the homomolecular dimers of H_2O, CO and NCCN, we employed the same geometries as were used in part I; therefore a direct comparison of the present results for the dispersion energy with those for the induction and electrostatic interaction energies becomes possible. For the urea dimer we studied additionally an assemblage of shifted parallel configurations that has been generated from a parallel geometry with a distance of 3·935 Å between the molecular planes by a parallel shift of one of the urea molecules. For the shift coordinate $S = \pm 3{\cdot}935$ Å the shifted geometries are identical with the structure PS as described in part I and depicted in fig. 4. Because all other dimer geometries have been described at length in part I, we repeat here only figures 1–4 and refer the reader for the details to [11].

For the numerical quadrature in equations (22) and (24) we used an M-point Gauss–Chebyshev integration scheme as proposed by Rijks and Wormer [45]

$$\int_0^\infty \mathrm{d}\omega S^{ab}(\omega)S^{ba}(\omega) = \sum_j^M W(\omega_j)S^{ab}(\omega_j)S^{ba}(\omega_j), \tag{31}$$

with

$$\omega_j = \cot\left(\pi\frac{2j-1}{4M}\right), \quad W(\omega_j) = \frac{2\pi}{4M\sin^2\left[\pi(2j-1)/4M\right]}. \tag{32}$$

In table 1 we have listed the dispersion energies as a function of the number of grid points M for two examples: the water dimer in an X-shaped geometry, calculated with a monocentred $1/R$ expansion, and for the cyanogen dimer in a parallel geometry, calculated with a four-site distributed $1/R$ expansion. As can be

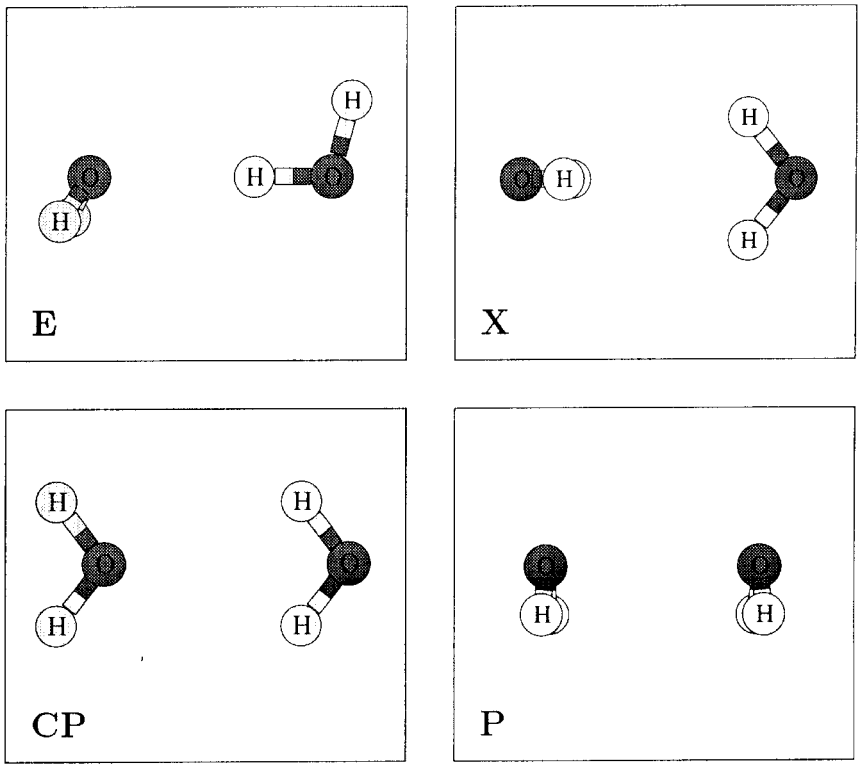


Figure 1. Orientations for the water dimer.

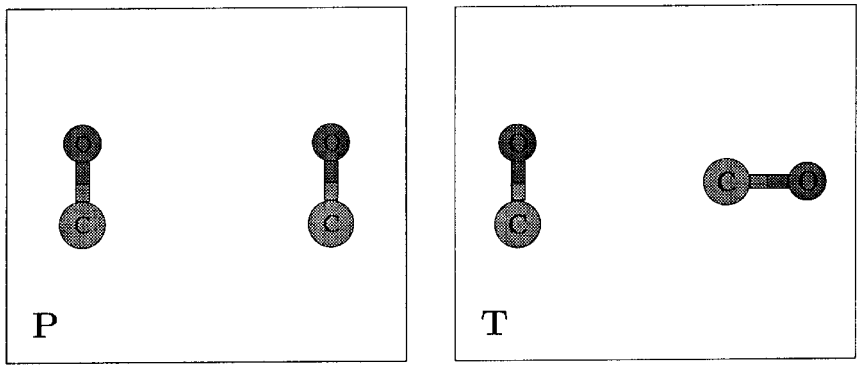


Figure 2. Orientations for the carbon monoxide dimer.

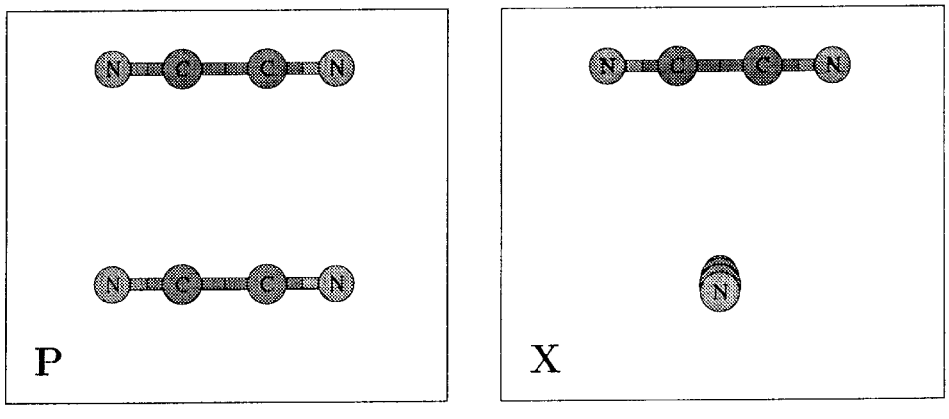


Figure 3. Orientations for the cyanogen dimer.

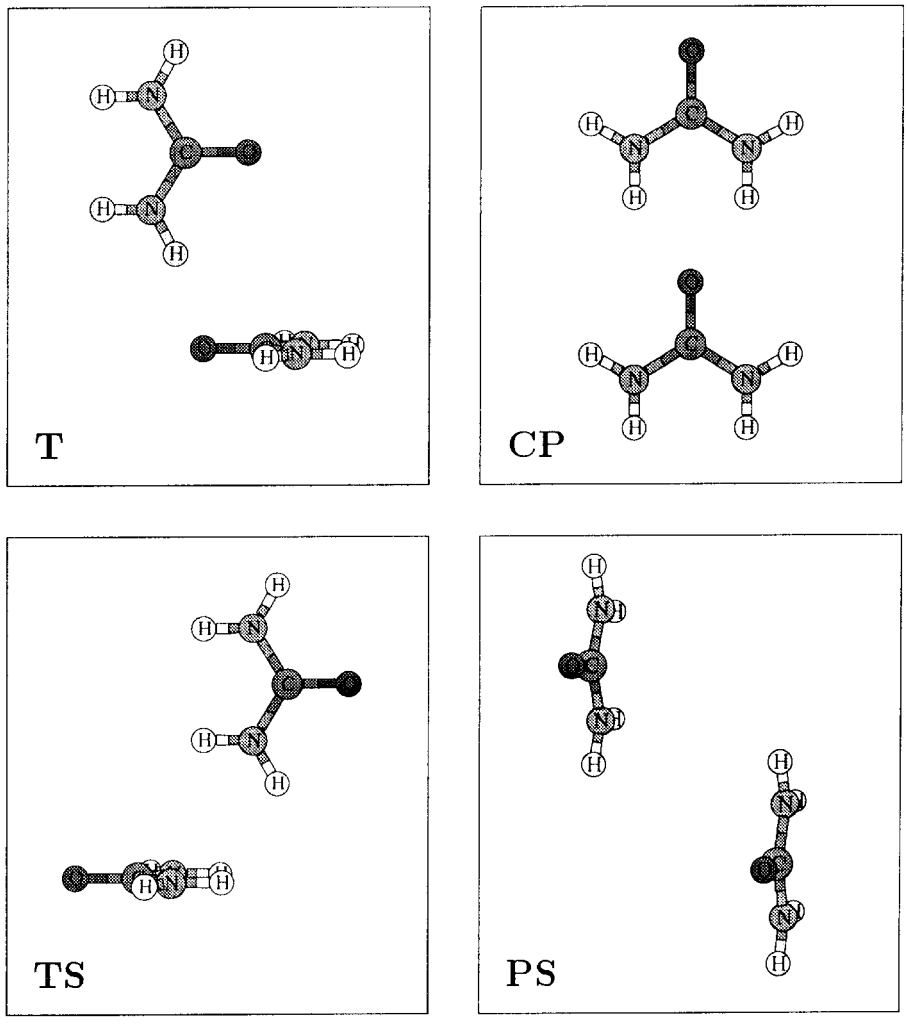


Figure 4. Orientations for the urea dimer.

Table 1. Dispersion energy as a function of the number of grid points in the Gauss–Chebyshev quadrature for the water dimer in orientation X at an O–O distance of 3·0 Å with a monocentred $1/R$ expansion of order 13 and for the cyanogen dimer in orientation P at an intermolecular distance of 3·5Å with a four-site distributed $1/R$ expansion of order 9.

Number of grid points	$H_2O \cdot H_2O$, orientation X		NCCN · CNNN, orientation P	
	E_{disp}/cm^{-1}	Relative error	E_{disp}/cm^{-1}	Relative error
2	- 839·420	5·6%	- 636·926	10·8%
3	- 879·502	1·1%	- 696·390	2·5%
4	- 886·981	0·2%	- 710·103	0·6%
5	- 888·526	5×10^{-4}	- 713·230	0·1%
6	- 888·871	1×10^{-4}	- 713·948	3×10^{-4}
7	- 888·952	3×10^{-5}	- 714·113	6×10^{-5}
8	- 888·971	6×10^{-6}	- 714·151	1×10^{-5}
9	- 888·975	$\approx 1 \times 10^{-6}$	- 714·158	$\approx 1 \times 10^{-6}$
10	- 888·976		- 714·159	

seen, this integration scheme leads to quickly convergent series for the dispersion energy, and with only ten integration points an accuracy of six digits is obtained. For most applications of multipole expansion, however, errors of the order of 1% and below will be insignificant and a Gauss–Chebyshev quadrature with three to five grid points would be sufficient. In all the following examples we used nevertheless ten grid points to ensure that the results are not affected by the accuracy of the numerical quadrature.

4. Results and discussion

4.1. *Maximum rank against* $1/R$ *expansion*

As discussed in section 2, a multipole expansion truncated at the order of the maximum tensor rank ('maximum-rank expansion' or 'L expansion') has the advantage with respect to the usual multipole expansion truncated at a given order of $1/R$ that not only does it guarantee negative induction and dispersion energies but also it is computationally more efficient, owing to a better factorization of the dispersion energy in equations (23) and (24) compared with the respective equations (21) and (22) for the expansion in orders N of $1/R$ (from here on also called the 'N expansion'). It is quite probable that the $1/R$ expansion leads to positive induction and dispersion energies only for extremely short intermolecular distances where the multipole expansion is not really valid; nevertheless, such an unphysical behaviour should also show some impact on the results for intermediate distances. In this range the multipole expansion converges only slowly or, to be more precise, it often approaches slowly a limiting value for the induction and dispersion energies before actual divergence is showing up.

As an example for the non-physical behaviour of the $1/R$ expansion let us mention the X-shaped configuration of the water dimer [11], where the induction energies of the ninth to thirteenth order in $1/R$ become positive for intermolecular distances below 2·5 Å. For the dispersion interaction, such an extreme failure has been detected only for very short distances, for example, for the urea dimer in geometry PS for distances of below 1·3 Å, where anyhow a multipole expansion becomes completely meaningless, irrespective of the number of expansion centres. Nevertheless, it appears that the L expansion scheme, beside its computational efficiency, has some significant advantages for the calculation of dispersion energies, if a multicentre expansion is employed.

In table 2 we compare the $1/R$ and the L expansion schemes for four selected configurations of the water dimer at a distance of R_{OO} = 3·0 Å between the oxygen atoms, as has already been done for the electrostatic and induction energies in part I. Concerning the maximum order N which can consistently be used in the calculation of $1/R$ expanded dispersion energies, exactly the same considerations hold as for the induction energy; N has to be reduced by three when using a distributed instead of a monocentre expansion, owing to the occurrence of charge-multipole polarizabilities.

Table 2. Dispersion energy for the water dimer in the orientations E, X, CP and P at R_{OO} = 3·0 Å as a function of the order N of $1/R$ (upper half) and the maximum rank L (lower half).

	E_{disp} /cm^{-1}							
	Orientation E		Orientation X		Orientation CP		Orientation P	
	Monocentred	Distributed	Monocentred	Distributed	Monocentred	Distributed	Monocentred	Distributed
N = 6	- 259	- 541	- 337	- 422	- 259	- 280	- 237	- 232
N = 7	- 294	- 640	- 430	- 486	- 259	- 313	- 227	- 236
N = 8	- 462	- 818	- 640	- 599	- 396	- 391	- 363	- 363
N = 9	- 541	- 904	- 683	- 643	- 396	- 409	- 363	- 366
N = 10	- 665		- 805		- 476		- 451	
N = 11	- 731		- 820		- 476		- 451	
N = 12	- 830		- 886		- 518		- 504	
N = 13	- 893		- 889		- 518		- 504	
L = 1	- 259	- 469	- 337	- 367	- 259	- 255	- 237	- 221
L = 2	- 512	- 827	- 745	- 614	- 440	- 411	- 416	- 325
L = 3	- 724	- 1381	- 1082	- 723	- 557	- 482	- 519	- 475
L = 4	- 947	- 1772	- 1148	- 764	- 617	- 504	- 553	- 559
L = 5	- 1076	- 1777	- 1088	- 801	- 595	- 512	- 557	- 586
L = 6	- 1142	- 3317	- 1012	- 853	- 566	- 525	- 550	- 586
L = 7	- 1196	- 59322	- 973	- 938	- 561	- 631	- 550	- 584
L = 8	- 1226		- 965		- 557		- 549	

Table 3. Dispersion energy for the water dimer in the orientations E, X, CP and P at R_{OO} = 3·5 Å as a function of the order N of $1/R$ (upper half) and the maximum rank L (lower half).

	E_{disp}/cm^{-1}							
	Orientation E		Orientation X		Orientation CP		Orientation P	
	Monocentred	Distributed	Monocentred	Distributed	Monocentred	Distributed	Monocentred	Distributed
N = 6	- 103	- 176	- 129	- 159	- 103	- 109	- 94	- 92
N = 7	- 114	- 194	- 159	- 179	- 103	- 119	- 94	- 94
N = 8	- 164	- 232	- 217	- 211	- 143	- 142	- 131	- 131
N = 8	- 183	- 241	- 227	- 222	- 143	- 146	- 131	- 131
N = 10	- 210		- 251		- 160		- 150	
N = 11	- 222		- 254		- 160		- 150	
N = 12	- 246		- 264		- 166		- 158	
N = 13	- 246		- 264		- 166		- 158	
L = 1	- 103	- 159	- 129	- 141	- 103	- 101	- 94	- 89
L = 2	- 174	- 231	- 239	- 213	- 152	- 145	- 143	- 119
L = 3	- 214	- 294	- 296	- 236	- 172	- 160	- 159	- 152
L = 4	- 247	- 305	- 295	- 245	- 178	- 163	- 161	- 164
L = 5	- 262	- 290	- 281	- 252	- 173	- 166	- 163	- 166
L = 6	- 268	- 284	- 273	- 257	- 171	- 167	- 163	- 165
L = 7	- 271	- 361	- 270	- 262	- 170	- 168	- 163	- 163
L = 8	- 273		- 270		- 170		- 163	

It should be noted that in the distributed case we used only up to 2^7-pole polarizabilities instead of up to 2^8-pole monocentred polarizabilities, so that the largest possible N of the distributed expansion becomes nine. Concentrating momentarily on the monocentred results, one can see advantages for the L expansion; allowing for 2^8-pole and 2^7-pole in addition to 2^6-pole polarizabilities changes the largest possible order of the $1/R$ expansion from N = 11 to N = 13, with corresponding energy changes in the order of about 10% or more, while the changes in the dispersion energies are only half that large when comparing L = 6 with L = 8 in the maximum-rank expansion. Table 2 does not allow one to draw similar conclusions for the distributed expansions, since the distributed maximum-rank expansion does not converge for orientations E, X and CP at R_{OO} = 3·0 Å. The corresponding numbers for an increased oxygen–oxygen distance of 3·5 Å are given in table 3. The maximum-rank expanded dispersion energy now is quite stable from L = 4 or 5 onwards (with the exception of orientation E; cf. section 4.2.1), while comparing the N = 7 with the N = 9 results for the $1/R$ expansion still shows significant energy changes.

We believe that the combined advantages of a simpler computational algorithm, the non-occurrence of unphysical sign changes, and an improved convergence behaviour make this the scheme of choice. Therefore we are going to consider exclusively the L expansion scheme in the following.

4.2. *Monocentred as against distributed multipole expansion*

4.2.1. *The water dimer*

The water monomer is a small molecule whose static dipole polarizability is highly isotropic; its mean polarizability is 9·92 au while the anisotropy is only 0·67 au [46]. According to our earlier findings [11], using the distributed three-site model did not lead to dramatic improvements in the convergence behaviour of the second-order induction energy for the water dimer. Hence, it is not surprising that the same is true for the dispersion energy. From the values in tables 2 and 3 and their graphical display in figure 5 it is hard to judge whether the distributed or the monocentred expansion is to be preferred at larger L values, with, however, the exceptions of orientation E and orientation CP at R_{OO} = 3·0 Å. In these cases the monocentred expansion seems to converge up to L = 8, while the distributed expansion clearly diverges in the end. In particular for orientation E, which at the shorter distance of 3·0 Å corresponds to the water dimer's approximate equilibrium geometry, one can observe the typical pattern of an asymptotically convergent series: first the distributed expansion seems to attain a limiting value for L = 4 - 5 (at R_{OO} = 3·0 Å) or 3–6 (R_{OO} = 3·5 Å) before it starts to diverge. It should be noted that the O...H distance in the hydrogen-bridged configuration E is about 1 Å shorter than R_{OO}. It is this small R_{OH} distance which enters into the distributed dispersion energy expression, while in the monocentred expression only the distance

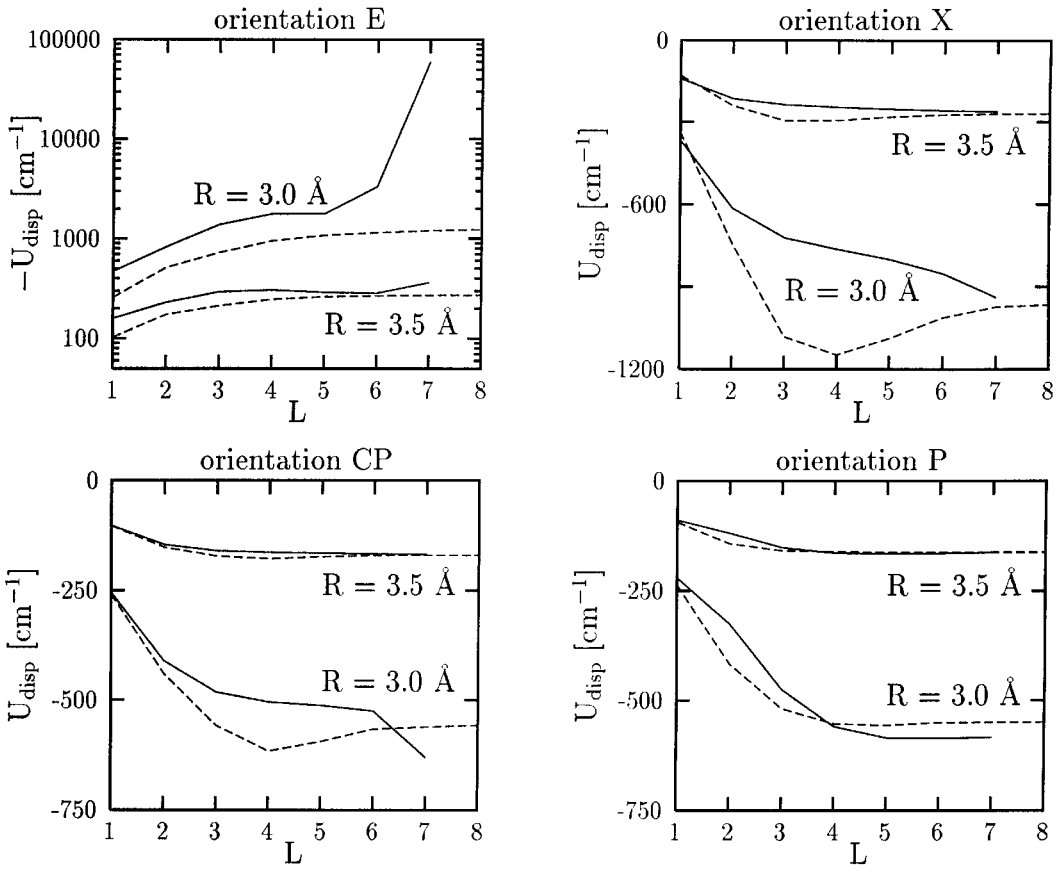


Figure 5. Dispersion energies U_{disp} for the water dimer as a function of the maximum rank L for several relative orientations and O–O distances R, where the interaction energies of different ranks are connected by straight lines to guide the eye: (——), distributed expansion; (– – –), monocentred expansions.

between the centres of mass of the molecules appears, the latter being nearly equal to R_{OO}. So, for the equilibrium configuration with R_{OO} = 3.0 Å, one finds that $1/R_{OH}$ is 50% larger than $1/R_{OO}$, meaning that a term such as $1/R_{OH}^{16}$ is about 650 times larger than $1/R_{OO}^{16}$. Terms with powers as large as 16 start to appear from L = 6 onwards, which explains the convergence problems of the distributed expansion in this case.

In the light of these results, one can conclude that the monocentred expansion is computationally more favourable than the three-site TPEP model for the calculation of the water dimers' dispersion energy.

4.2.2. *The carbon monoxide dimer*

Parallel (P) and T-shaped (T) orientations as well as an in-plane rotation of one of the CO monomers about its geometrical centre transforming the dimer from orientation P to T (cf. figure 2) have been investigated in the case of $(CO)_2$. In figure 6, dispersion energies obtained by monocentred and distributed multipole expansions are plotted against the rotation angle Θ for a fixed distance R = 3·5 Å between the centres of mass. $\Theta = 0^\circ$ corresponds to orientation P and $\Theta = 270^\circ$ to orientation T. A behaviour similar to that of the water dimer in the orientation E has been found for the rotation. After a fast convergence, the distributed expansion attains a limiting value for L = 3- 4 and remains stable for L = 4- 6. The divergence of the distributed multipole expansion for L = 7 can be seen by an unphysical anisotropy, manifested by strong undulations of the corresponding curve in figure 6. Convergence is much slower for the monocentred expansion, and at least L = 4 is needed to obtain a reasonable approximation for the dispersion energy. Again, the monocentred expansion remains stable up to L = 7 and 8. The results for L = 8 are not displayed in figure 6 because they differ for all angles by less than 5 cm^{-1} from the results for L = 7. The relatively good performance of the distributed expansion for the CO dimer is exemplified by figure 7, which shows for both selected orientations the fast convergence of the distributed expansion to a limiting value. With L = 3 the two-site TPEP model yields very good accuracy with deviations of less than 40 cm^{-1} from the results for L = 6 for all angles. To achieve a

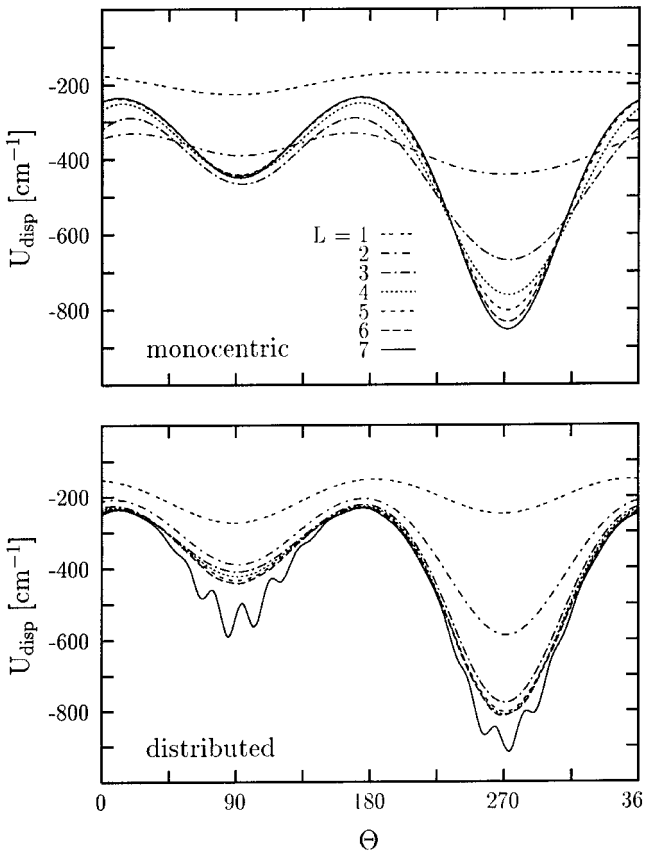


Figure 6. Monocentred and distributed dispersion energies U_{disp} of the carbon monoxide dimer as a function of the angle Θ between the two molecular axes for an in-plane rotation of one CO monomer about its geometrical centre, at a fixed distance of 3·5 Å between the centres. $\Theta = 0^{\circ}$ corresponds to orientation P, and $\Theta = 270^{\circ}$ to orientation T (cf. figure 2). Monocentred interaction energies of rank $L = 8$ are not displayed since they are almost indistinguishable from those of rank 7.

similar accuracy with the monocentred expansion requires a maximum rank of at least $L = 5$. For a two-site model with $L = 3$ the product $N_{cent} \times N_{comp}$ is $2 \times 9 = 18$ while, for a monocentred expansion with $L = 5$, one has 24 multipole components to consider. Thus from a computational point of view the two-site model should be favoured, as far as the accuracy obtained with $L = 3$ is sufficient. If higher accuracy is required, a monocentred expansion will be more efficient.

4.2.3. *The cyanogen dimer*

The homomolecular dimers of water and carbon monoxide are two examples, for which the interatomic distances within the monomers are much smaller than any intermolecular atom–atom distance, at least for all physically relevant dimer geometries. Therefore the necessary convergence condition of the monocentred expansion, that the spheres drawn around the molecular expansion centres which include all atoms of the respective monomer do not touch or overlap, was always fulfilled. The next example that we are going to study is the cyanogen dimer, that is, a dimer composed of strongly non-spherical monomers, for which the convergence condition is violated in large regions of the potential energy (hyper)surface accessible by the van der Waals complex.

The parallel (P) and the X-shaped geometries of the cyanogen dimer provide spectacular examples for the catastrophic divergence of monocentred multipole expansions in this case (figure 8). The monomer is about 3·69 Å long; thus two spheres containing the monomers do not overlap for an intermolecular distance $R = 4{\cdot}5$ Å, while for $R = 3{\cdot}5$ Å the convergence condition for the monocentred expansion is violated. As can be seen from figure 8, the distributed dispersion energy calculated from the dynamic TPEP polarizabilities converges neatly for both distances in both orientation P and orientation X. A good approximation for the limiting value, reached at $L = 7$ (as for the CO dimer), is already obtained with $L = 4$. This is in sharp contrast with the monocentred expansion, which diverges rapidly for the shorter distance and becomes unstable from $L = 6$ onwards already for $R = 4{\cdot}5$ Å in orientation P.

Even if Tang–Toennies-like [10] damping functions were employed it would be doubtful whether the monocentred expansion is able to yield reasonable dispersion energies for the cyanogen dimer, while the distributed expansion using dynamic TPEP polarizabilities has a completely satisfactory convergence behaviour at least up to $L = 7$. This expansion is supposed to lead to reliable dispersion energies if the higher-order terms of the asymptotic series are damped with a suitable *Ansatz*.

4.2.4. *The urea dimer*

We investigated four structures of the urea dimer that correspond to pairs of nearest and second-nearest neighbours in the urea crystal, as described in part I. A sphere around the centre of mass of the urea molecule which contains all nuclei has a radius of 2·03 Å. These spheres do not overlap for either of the four nearest- and second-nearest-neighbour pairs in the urea crystal. Thus, for the crystal dimer geometries, no decisive advantage can be expected from the use of distributed polarizabilities to calculate the dispersion energy. Figure 9 shows that for geometries T and CP we encounter the same convergence problems as for the hydrogen-bridged water dimer orientation E (see section 4.2.1), owing to the short intermolecular O…H distances of 1·99 and 2·06 Å; the distributed expansion first approaches a similar limit as the monocentred expansion before it

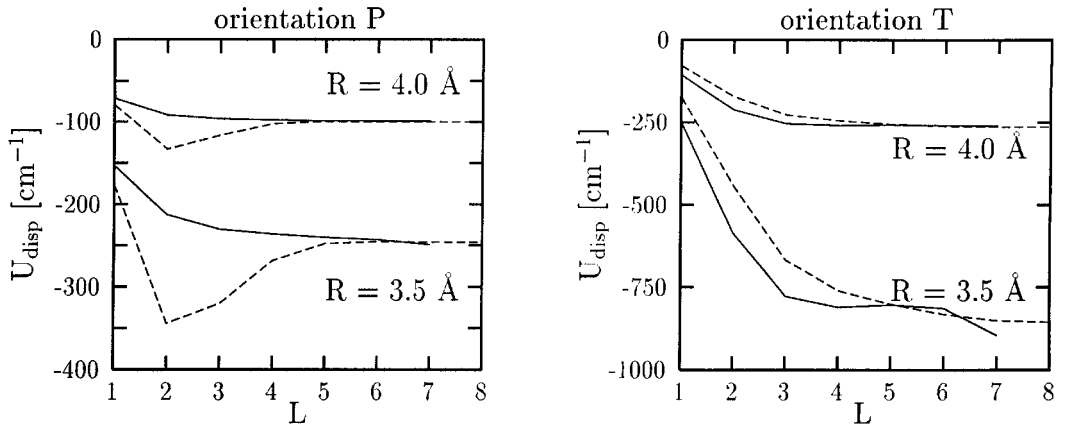


Figure 7. Dispersion energies U_{disp} for the carbon monoxide dimer as a function of the maximum rank L for the two orientations P and T (cf. figure 2) and two different distances R between the geometrical centres of the monomers: (——), distributed expansion; (– – –), monocentred expansion.

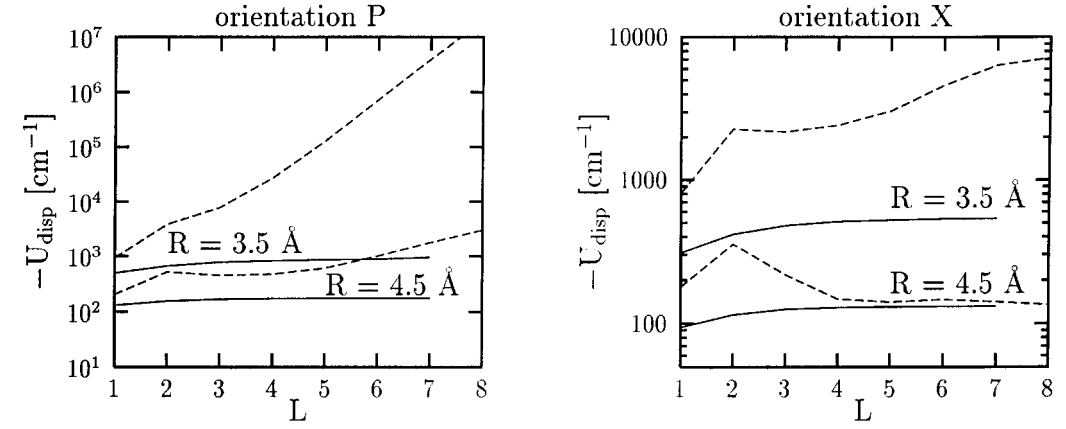


Figure 8. Dispersion energies U_{disp} for the cyanogen dimer as a function of the maximum rank L for the two orientations P and X (cf. figure 3) and two different distances R between the geometrical centres of the monomers: (——), distributed expansion; (– – –), monocentred expansion.

starts to diverge rapidly. The monocentred expansion is quite stable up to $L = 8$ for geometry T, but for geometry CP it becomes unstable at $L = 7$. For geometry TS neither of the two expansions shows satisfactory convergence behaviour. The distributed as well as the monocentred expansions converge nicely only in the case of the shifted parallel configuration PS.

We studied also a set of parallel shifted configurations where one urea monomer has been shifted in a plane 3·935 Å above the molecular plane of the other monomer. For the shift coordinate $S = 0{\cdot}0$ Å this corresponds to one urea molecule exactly on top of the other, the two molecular planes in parallel and both molecules in the same orientation; for $S = \pm 3{\cdot}935$ Å, one obtains the dimer geometries PS actually found in the crystal. In figure 10, the dispersion energies for the shifted parallel geometries are plotted as continuous functions of the shifting coordinate S. As mentioned above, for this geometry the molecular spheres do not overlap and, because no extremely short intermolecular atom–atom distance occurs, both expansions have a stable convergence behaviour up to the highest maximum rank considered. If the absolute value of the shifting coordinate S is reduced, the molecular spheres approach and start to overlap at $S \approx \pm 1$ Å. As can be seen from figure 10 the distributed expansion remains completely stable over the whole range of S, while for the monocentred expansion the convergence is spoiled as soon as the spheres approach. In fact, for $|S| < 2{\cdot}0$ Å the monocentred expansion becomes increasingly unstable and clearly diverges for $S = 0{\cdot}0$ Å.

5. Conclusions

The results obtained for the four homomolecular dimers considered in the present study show that it is possible to solve the shape convergence problem for

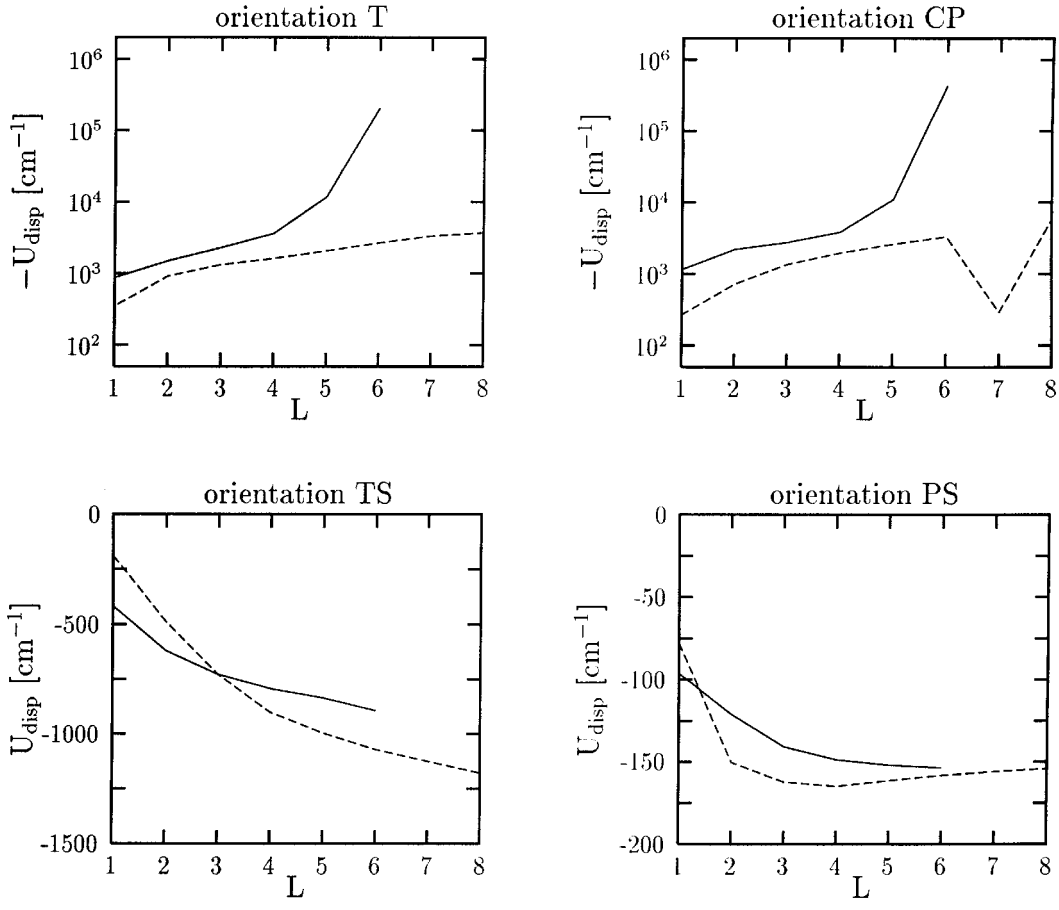


Figure 9. Dispersion energies U_{disp} for the urea dimer as a function of the maximum rank L for several pair geometries in the urea crystal: (——), distributed expansion; (– – –), monocentred expansion.

multipole expanded dispersion energies using distributed dynamic polarizabilities. In particular, the topological partitioning of the charge-density susceptibility function, developed in [23] provides a suitable *a-priori ab-initio* scheme to calculate distributed frequency-dependent polarizabilities that lead to induction and dispersion interaction energies with reasonably stable convergence properties.

Distributed expansions are comparable with monocentred expansions, however, in that they are also based on point multipole–multipole polarizabilities. For this reason, distributing multipoles is not sufficient to transform the asymptotically convergent monocentred multipole series into a truly convergent series. That any point–multipole expansion, be it monocentred or distributed, is only asymptotically convergent is due to the exponential decrease in the charge–density susceptibility function which extends to infinity and thus in principle cannot be properly described by a 'point' multipole expansion. The resulting extension convergence problem probably can be solved by application of a suitable damping scheme.

As can be seen from two striking examples, the cyanogen dimer and the parallel shifted geometries of the urea dimer, a distributed expansion using TPEPs reduces the convergence problem of the monocentred expansion to an atom-wise extension problem dominated by the shortest intermolecular atom–atom distances. It was demonstrated in part I [11] of this study that this is also the case for the first-order electrostatic and for the second-order induction energy. Thus we are optimistic that the topological partitioning of electric properties in combination with a reasonable *Ansatz* for damping functions and for the exchange-overlap repulsion will open the possibility to calculate accurate potential energy hypersurfaces for weakly bound complexes of large and non-spherical molecules. Whether this will be possible for hydrogen-bonded complexes is not yet clear from the present results. In these cases, extremely short intermolecular atom–atom distances occur and the limit of the damped multipole series for the interaction energies will become very sensitive to the choice of the damping functions. In any case, it is clear that a global damping function will not be appropriate

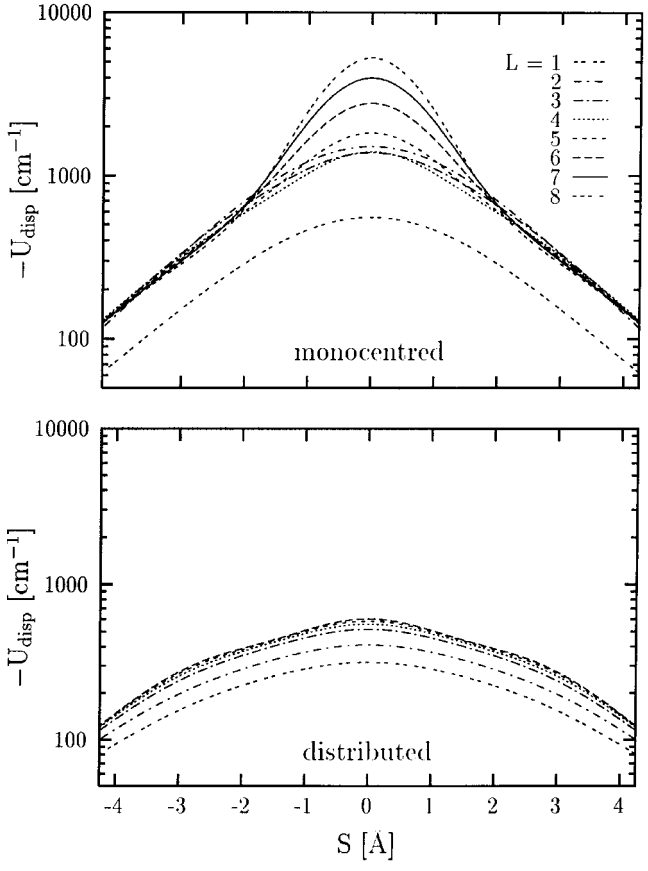


Figure 10. Dispersion energies U_{disp} for the urea dimer in paralel shifted geometries as a function of the shifting coordinate S. S = 0 Å corresponds to a parallel structure with a distance of 3·935 Å between the molecular planes of the monomers, and $S = \pm 3{\cdot}935$ Å corresponds to geometry PS (cf. figure 4).

and that instead a different damping function will have to be used for each rank L.

G.J. is indebted to the Humboldt Foundation (Bonn) for a Feodor Lynen fellowship and to the CNRS. C.H. and B.A.H. thank the Deutsche Forschungsgemeinschaft for financial support of this work through the Sonderforschungsbereich 334.

References

[1] van Lenthe, J. H., van Duijneveldt-van de Rijdt, J. G. C. M., and van Duijneveldt, F. B., 1987, *Adv. chem. Phys.*, **69,** 521.
[2] Chałasiński, G., and Szczęśniak, M. M., 1994, *Chem. Rev.*, **94,** 1723.
[3] Magnasco, V., and McWeeny, R., 1991, *Theoretical Models of Chemical Bonding*, Part 4, edited by Z. B. Maksić (Berlin: Springer).
[4] Jeziorski, B., Moszynski, R., and Szalewicz, K., 1994, *Chem. Rev.*, **94,** 1887.
[5] Smirnov, B. M., and Chibisov, M. I., 1965, *Soviet Phys. JETP*, **21,** 624.
[6] Duman, E. L., and Smirnov, B. M., 1970, *Opt. Spectrosc.*, **29,** 229.
[7] Ahlrichs, R., Penco, R., and Scoles, G., 1977, *Chem. Phys.*, **19,** 119.
[8] Koida, A., 1976, *J. Phys.*, **9,** 3173.
[9] Feltgen, R., 1981, *J. chem. Phys.*, **74,** 1186.
[10] Tang, K. T., and Toenies, J. P., 1984, *J. chem. Phys.*, **80,** 3726.
[11] Jansen, G., Hättig, C., Hess, B. A., and Ángyán, J. G., 1996 , *Molec. Phys.*, **88,** 69.
[12] Stone, A. J., 1981, *Chem. Phys. Lett.*, **83,** 233.
[13] Sokalski, W. A., and Poirier, R. A., 1983, *Chem. Phys. Lett.*, **98,** 86.
[14] Vigné-Maeder, F., and Claverie, P., 1988, *J. chem. Phys.*, **88,** 4934.
[15] Dalgarno, A., and Lewis, J. T., 1955, *Proc. R. Soc.* A, **233,** 70.
[16] Young, R. H., 1975, *Int. J. quantum. Chem.*, **9,** 47.
[17] Ahlrichs, R., 1976, *Theor. chim. Acta*, **41,** 7.
[18] Brezin, E., and Zinn-Justin, J., 1979, *J. Phys. Lett., Paris*, **40,** L-511.
[19] Morgan, J. D., III, and Simon, B., 1980, *Int. J. quant. Chem.*, **17,** 1143.
[20] Cizek, J., Clay, M. R., and Paldus, J., 1980, *Phys. Rev.* A, **22,** 793.
[21] Wheatley, R. J., 1993, *Molec. Phys.*, **79,** 597.
[22] Le Sueur, C. R., and Stone, A. J., 1993, *Molec. Phys.*, **78,** 1267.
[23] Ángyán, J. G., Jansen, G., Loos, M., Hättig, C., and Hess, B. A., 1994, *Chem. Phys. Lett.*, **219,** 267.
[24] Bader, R. F. W., 1991, *Chem. Rev.*, **91,** 893.
[25] Bader, R. W. F., 1990, *Atoms in Molecules—A Quantum Theory* (Oxford University Press).
[26] Casimir, H. B. G., and Polder, D., 1948, *Phys. Rev.*, **73,** 360.
[27] McWeeny, R., 1992, *Methods of Molecular Quantum Chemistry*, second edition (London: Academic Press).
[28] Stone, A. J., 1991, *Theoretical Models of Chemical Bonding*, Part 4, edited by Z. N. Maksić (Berlin: Springer).
[29] Hättig, C., and Hess, B. A., 1994, *Molec. Phys.*, **81,** 813.
[30] Wormer, P. E. S., 1975, Thesis, University of Nijmegen.
[31] Visser, F., Wormer, P. E. S., and Stam, P., 1983, *J. chem. Phys.*, **79,** 4973.
[32] Pack, R. T., 1976, *J. chem. Phys.*, **64,** 1659.
[33] Hättig, C., 1996, *Chem. Phys. Lett.*, **260,** 341.
[34] Stolarczyk, L. Z., and Piela, L., 1979, *Int. J. quant. Chem.*, **15,** 701.
[35] Sadlej, A. J., 1988, *Collect. Czech. chem. Commun.*, **53,** 1995.
[36] Benedict, W. S., Gailar, N., and Plyler, E. K., 1956, *J. chem. Phys.*, **24,** 1139.
[37] Huber, K. P., and Herzberg, G., 1979, *Constants of Diatomic Molecules*, Vol. 4, *Molecular Spectra and Molecular Structure* (Princeton, New Jersey: Van Nostrand).
[38] Herzberg, G., 1966, *Electronic Spectra and Electronic Structure of Polyatomic Molecules*, Vol. 3, *Molecular Spectra and Molecular Structure* (Princeton, New Jersey: Van Nostrand).
[39] Swaminathan, S., Craven, B. M., and McMullan, R. K., 1984, *Acta crystallogr.* B, **40,** 300.

[40] Cioslowski, J., 1996, *Molec. Phys.*, **88,** 621.
[41] Biegler-König, F. W., Bader, R. W. F., and Tang, T. H., 1982, *J. comput. Chem.*, **3,** 317.
[42] Jansen, G., Hättig, C., and Ángyán, J. G., 1994, *CAUCHY—A TDHF Program for Distributed Polarizabilities.*
[43] Hättig, C., 1994, *FOURIER—A TDHF/TDMP2 Program.*
[44] Anderson, K., Blomberg, M. R. A., Fülsscher, M. P., Lindh, R., Malmquist, P.-Å., Olsen, J., Roos, B. O., Sadlej, A. J., and Widmark, P.-O., 1992, *MOLCAS version 2* (University of Lund).
[45] Rijks, W., and Wormer, P. E. S., 1988, *J. chem. Phys.*, **88,** 5704.
[46] Murphy, W., 1977, *J. chem. Phys.*, **67,** 5877.